INTERCOMPARISON OF 4 YEARS OF GLOBAL FORMALDEHYDE OBSERVATIONS FROM THE GOME-2 AND OMI SENSORS

Isabelle De Smedt[1], Michel Van Roozendael[1], Trissevgeni Stavrakou[1], Jean-François Müller[1], Kelly Chance[2], Thomas Kurosu[3].

[(1)] Belgian Institute for Space Aeronomy (BIRA-IASB), Avenue circulaire, 3, B-1180 Brussels, Belgium, isabelle.desmedt@aeronomie.be
[(2)] Harvard-Smithsonian Center For Astrophysics, Smithsonian Astrophysical Observatory (CFA-SAO), United-States.
[(3)] Jet Propulsion Laboratory (JPL), California Institute of Technology, United-States.

ABSTRACT

Formaldehyde (H_2CO) tropospheric columns have been retrieved since 2007 from backscattered UV radiance measurements performed by the GOME-2 instrument on the EUMETSAT METOP-A platform. This data set extends the successful time-series of global H_2CO observations established with GOME/ ERS-2 (1996-2003), SCIAMACHY/ ENVISAT (2003-2012), and OMI on the NASA AURA platform (2005-now). In this work, we perform an intercomparison of the H_2CO tropospheric columns retrieved from GOME-2 and OMI between 2007 and 2010, respectively at BIRA-IASB and at Harvard SAO. We first compare the global formaldehyde data products that are provided by each retrieval group. We then investigate each step of the retrieval procedure: the slant column fitting, the reference sector correction and the air mass factor calculation. New air mass factors are computed for OMI using external parameters consistent with those used for GOME-2. By doing so, the impacts of the different a priori profiles and aerosol corrections are quantified. The remaining differences are evaluated in view of the expected diurnal variations of the formaldehyde concentrations, based on ground-based measurements performed in the Beijing area.

1. SATELLITE H_2CO PRODUCTS

Satellite formaldehyde columns are retrieved in the near ultraviolet using the differential optical absorption spectroscopy (DOAS) technique (Platt and Stutz, 2008) which involves two main steps. First, the effective slant column amounts (corresponding to the integrated H_2CO concentrations along the mean atmospheric optical path) are derived through least-squares fits of the measured Earth reflectance spectra to laboratory absorption cross-sections. Second, the slant columns are converted into vertical columns by means of an air mass factors obtained from suitable radiative transfer calculations, accounting for the presence of clouds and aerosols, surface properties and best-guess H_2CO vertical profiles. A third step is performed in the case of formaldehyde, which consists in a normalisation of the columns in a reference sector, chosen as the remote Pacific Ocean. The method of Palmer et al. (2001) is used for the calculation of the tropospheric air mass factors. It consists in separating the scattering properties of the atmosphere, described with the so-called scattering weighting functions, and the vertical distribution of formaldehyde, described by the profile shapes.

The H_2CO vertical columns are obtained using the following equation: $VC = \frac{\Delta SC}{AMF} + VC_0^{CTM}$, where ΔSC is the differential slant column, AMF is the tropospheric air mass factor and VC_0^{CTM} is the H_2CO background obtained from a tropospheric model in the reference sector.

1.1. H_2CO GOME-2 v12

The GOME-2 H_2CO product (v12) developed at BIRA-IASB is described in details in De Smedt et al. (2012) and available on the TEMIS website (http://h2co.aeronomy.be). Briefly, the slant columns are retrieved in the 328.5-346 nm wavelength range, using the H_2CO absorption cross-sections of Meller and Moortgat (2000). For the air mass factor calculation, the a priori H_2CO profile shapes are taken from the IMAGESv2 3D-CTM (daily morning profiles with a spatial resolution of 2x2.5°). The scattering weighting functions are evaluated with the LIDORT v3.0 radiative transfer model (Spurr, 2008) at 340 nm. The surface reflectivity is taken from the OMI monthly albedo climatology of Kleipool et al. (2008) at 342 nm, with a spatial resolution of 0.5°. The cloud product is the version 6 of the FRESCO algorithm, which provides an effective cloud fraction and cloud top height assuming a Lambertian-reflecting cloud with an albedo of 0.8 (Wang et al., 2008). In the case of cloudy scenes, a correction is applied using the independent pixel approximation (Martin et al., 2002). No explicit correction is applied for aerosols. Consistent retrieval settings are used for the GOME and

Proc. of 'ATMOS 2012 – Advances in Atmospheric Science and Applications', Bruges, Belgium (ESA SP-708, November 2012)

SCIAMACHY H_2CO products, in order to ensure full consistency between the time series (De Smedt et al., 2008 and 2012).

1.2. NASA OMI v2.0 collection 3

The OMI H_2CO product (v2.0, collection 3) developed at Harvard-SAO is described in Kurosu et al. (2008) and is provided via the NASA/mirador website (http://mirador.gsfc.nasa.gov/). The slant columns are retrieved in a large fitting interval, 327.5-356.5 nm, using the H_2CO absorption cross-sections of Meller and Moortgat (2000). For the air mass factor calculation, the a priori H_2CO profile shapes are taken from GEOS-CHEM (monthly profiles with a spatial resolution of 2x2.5°). The scattering weighting functions are also evaluated with the LIDORT v3.0 radiative transfer model (Spurr, 2008), but at 328 nm. Like for the GOME-2 product, the surface reflectivity is taken from the monthly albedo climatology of Kleipool et al. (2008). The OMI cloud product is retrieved from the O_2-O_2 absorption band, also assuming a Lambertian-reflecting cloud with an albedo of 0.8 (Stamnes et al., 2008). Also like the GOME-2 product, the independent pixel approximation is used to correct for cloudy observations (Martin et al., 2002). Furthermore, the aerosol optical effects are corrected using extinction profile from the GEOS-CHEM model (Martin et al., 2003).

Figures 1 and 2 present maps of formaldehyde vertical columns, averaged over the period 2007-2008, respectively from the GOME-2 and OMI products. Over the continents, the NASA OMI v2.0 columns present systematically lower values than the GOME-2 observations. As the reference sector correction is the same for both products, in the next sections we look for the reason of this discrepancy by comparing separately the GOME-2 and OMI differential slant columns and air mass factors.

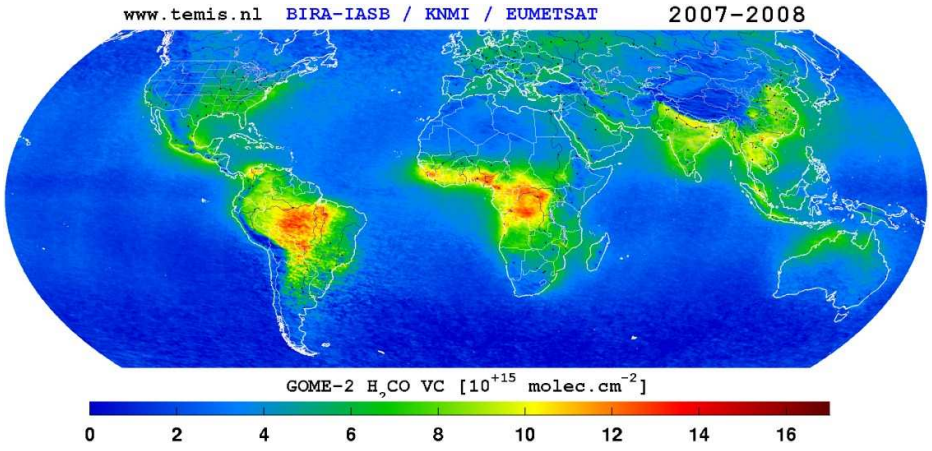

Figure 1: H_2CO vertical column retrieved from GOME-2 spectra between 2007 and 2008 (De Smedt et al., 2012).

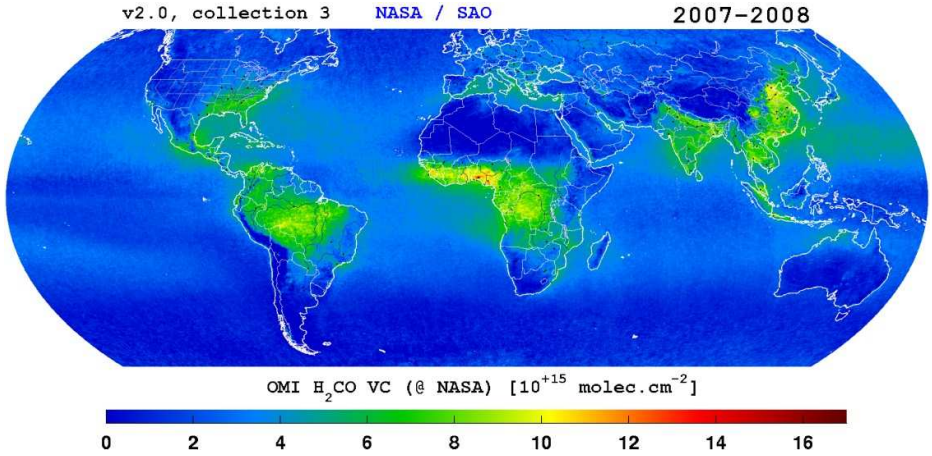

Figure 2: H_2CO vertical column retrieved from OMI between 2007 and 2008 (Kurosu et al., 2008).

2. SLANT COLUMNS

2.1. Random noise of the slant columns

The random noise of the GOME, SCIAMACHY, GOME-2 and OMI H_2CO measurements are compared in Figure 3, as an indication of the quality of the fits. For this figure, the standard deviation of the differential slant columns in the clean equatorial Pacific has been analysed over the entire time period of measurements for each instrument. In this area, one can assume that the H_2CO production due to NMVOC oxidation can be neglected, and that the daily variations of the CH_4 oxidation are weak. The standard deviation of the retrieved H_2CO columns is therefore a measure of the random noise of the measurements. In order to compare the instrument performances, the standard deviations have been corrected for each pixel area and scaled to a common pixel area of $10x10km^2$. Since GOME, SCIAMACHY and GOME-2 have similar instrumental designs, and since the H_2CO retrieval settings have been aligned, differences in the standard deviations on the retrieved slant columns are equivalent and proportional to the square root of the different instrument ground pixel areas (De Smedt et al., 2008 and 2012). Because the OMI instrument provides measurements with a better signal to noise ratio than the European sensors, and because the fitting interval used to retrieve H_2CO is larger, the random noise of the OMI H_2CO columns is twice smaller than the GOME-2 columns (brought back to a common ground pixel size).

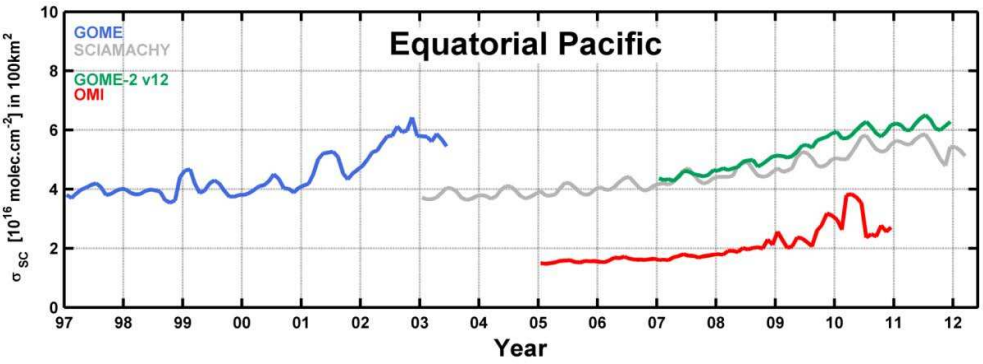

Figure 3: Random noise of the H_2CO slant columns retrieved from GOME, SCIAMACHY, GOME-2 and OMI spectra, for a common pixel size of 10x10 km².

2.2 Differential slant columns

Figure 4 compares the H_2CO differential slant columns of SCIAMACHY (grey line), GOME-2 (green line) and OMI (red line), averaged at the global scale, separately over the continents and over the seas. As a direct result of the reference sector correction, the mean differential slant columns over the seas are found very close to zero for the three products. Over the continents however, the OMI columns present a global negative offset of about $2.5x10^{15}$ molec.cm^2 compared to the SCIAMACHY and GOME-2 H_2CO columns. Furthermore, the annual averages of the OMI H_2CO differential slant columns (given inset each plot) are of the same order of magnitude over the continents and over the seas (from 0 to $9x10^{14}$ molec.cm^{-2}). This feature is not expected from the formaldehyde columns. Indeed, above a global and well mixed background due to methane oxidation, the main source of H_2CO is the oxidation of NMVOCs, resulting in important and localised enhancements of the H_2CO concentration over the continents. Figure 5 shows the H_2CO differential slant columns averaged over four important regions of emissions: Southeastern US, Northern China, Amazonia and Southern Africa. While the SCIAMACHY and GOME-2 columns are roughly consistent, the OMI values are systematically lower, by a magnitude depending on the region and on the year. These systematic differences are probably related to the different settings used to fit the slant columns, particularly the fitting windows, but more tests are needed to draw conclusions about the quality of the slant columns. In the rest of the present work, we simply add an offset of $2.5x10^{15}$ molec.cm^2 to the OMI differential slant columns over the continents.

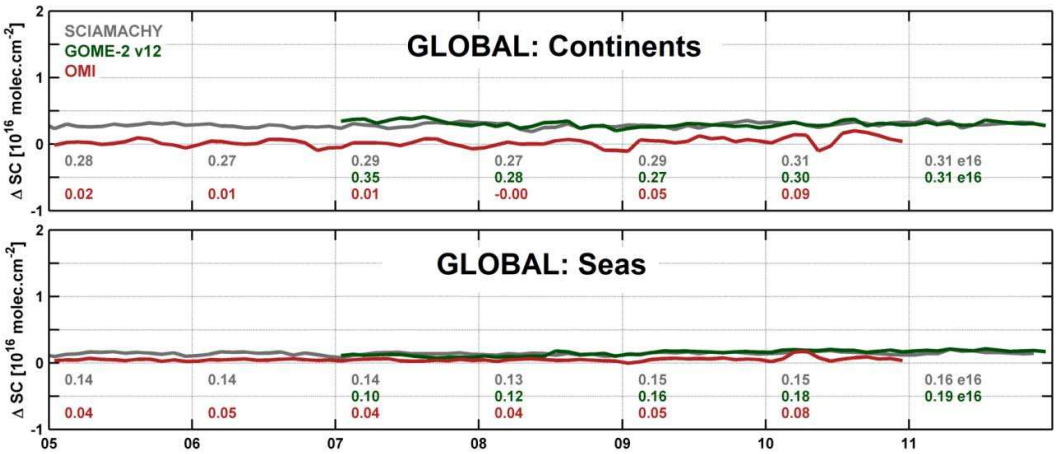

Figure 4: Global averages of the SCIAMACHY, GOME-2 and OMI H_2CO differential slant columns, calculated over continents (upper panel) and over seas (lower panel). Annual values are given at the bottom of each subplot for each instrument [10^{16} molec.cm^{-2}].

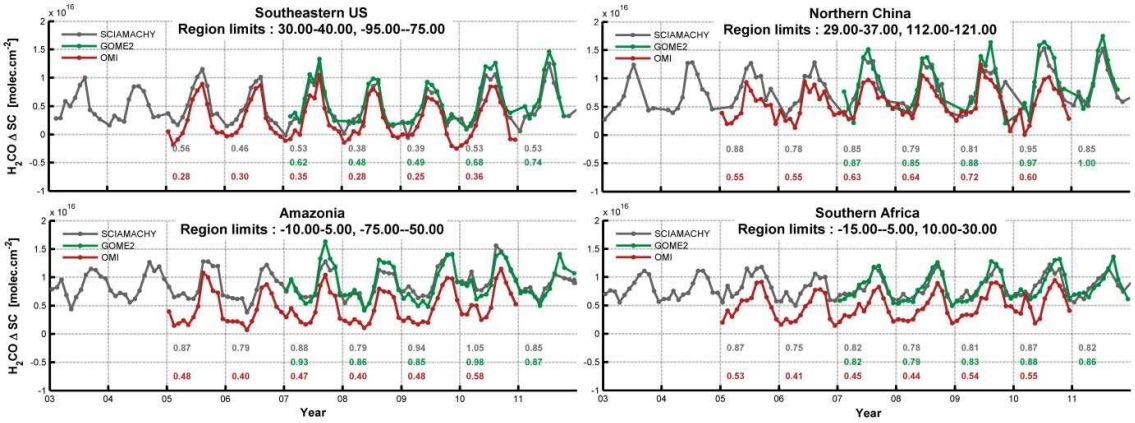

Figure 5: Regional averages of the SCIAMACHY, GOME-2 and OMI H_2CO differential slant columns, calculated over Southeastern US, Northern China, Amazonia and Southern Africa. Annual values are given at the bottom of each subplot for each instrument [10^{16} molec.cm^{-2}].

3. AIR MASS FACTORS

Figure 6 presents a comparison of the air mass factors of the SCIAMACHY (SCIA BISA, grey line), GOME-2 (GOME-2 BISA, green line) and OMI (OMI NASA, dotted red line) products in the same regions as Figure 5. Furthermore, new AMF are shown for OMI (OMI BISA, red line). They have been calculated at BIRA-IASB, using parameters consistent with the SCIAMACHY and GOME-2 products. The H_2CO profile shapes are taken from the IMAGESv2 model (daily afternoon profiles, with a spatial resolution of 2x2.5°). The scattering weights are simulated with LIDORT at 340 nm. The albedo and cloud products remain the same, as well as the cloud correction. No explicit correction is applied for aerosols, contrary to the NASA OMI product.

We observe that the AMFs are systematically lower for the OMI observation geometry than for the GOME-2 geometry (both for BISA and NASA OMI AMFs). In Southeastern US, Amazonia and Africa, the NASA and BISA AMFs are pretty close, the NASA AMFs being higher by about 5 to 10%. This difference is explained for its largest part by the different wavelengths used to perform the radiative transfer calculations, the AMFs calculated at 340 nm being 5 to 10% larger than at 328 nm. The a priori profile shapes are very similar between the IMAGES and GEOS-CHEM models (not shown), and therefore do not have an important impact on the new air mass factors. Note however that uncertainties of the H_2CO profile shapes do have important systematic impact on the final vertical columns. The correction for aerosols in the NASA product has localised effects, for example in Northern China in winter, where the NASA AMFs are about 30% lower than the BISA AMFs for OMI.

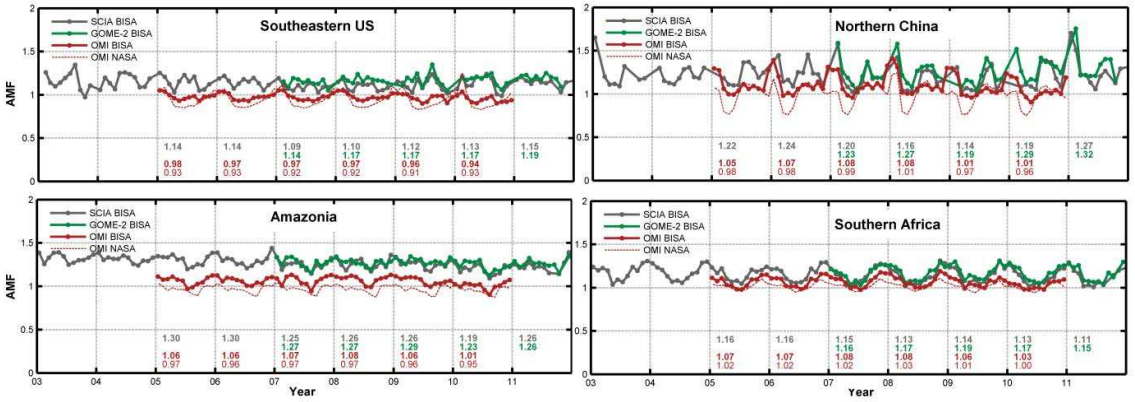

Figure 6: Regional averages of the SCIAMACHY, GOME-2 and OMI H_2CO air mass factors, over Southeastern US, Northern China, Amazonia and Southern Africa. Two versions are shown for the OMI AMFs: the AMFs provided in the NASA product (OMI NASA, dotted red line), and the AMF calculated at BIRA-IASB (OMI BISA, red line) with settings consistent with the SCIAMACHY and GOME-2 H_2CO products. Annual values are given at the bottom of each subplot for each instrument [no unit].

4. VERTICAL COLUMNS

The final vertical columns are compared in Figure 7. The NASA OMI vertical columns are shown in dotted red line. New vertical columns for OMI are also shown (OMI BISA, red line). They have been calculated at BIRA-IASB, starting from the NASA differential slant columns, but using BISA AMFs (see section 3) and adding a continental offset of $2.5x10^{15}$ molec.cm^{-2} (see section 2):

$$VC_{BISA} = \frac{\Delta SC_{NASA}}{AMF_{BISA}} + VC_0^{CTM} + 2.5x10^{15}.$$

Although the correlation coefficient between the OMI and GOME-2 vertical columns were already high (from 0.79 to 0.93), they are improved by the new settings in the four regions (from 0.84 to 0.96). Furthermore, the final agreement between the BISA OMI and GOME-2 vertical columns is very satisfactory in Southeastern US, Amazonia and Southern Africa, with regression lines presenting offsets lower than $5x10^{14}$ molec.cm^{-2} and slopes diverging by less than 15% from unity. In Northern China, the agreement of the OMI vertical columns with the GOME-2 observations is not improved by the BISA corrections. The OMI_{BISA} columns present a significant positive offset of almost $4x10^{15}$ molec.cm^{-2}, and a slope of -27% compared to the GOME-2 columns. However, these differences may be explained by the diurnal variation of the formaldehyde columns in this region (see next section).

The good final agreement between GOME-2 and OMI H_2CO VC can also be seen on Figure 8, presenting seasonal averages of the GOME-2 and OMI_{BISA} H_2CO vertical columns between 2007 and 2010. In comparison to Figure 1, the improvement is obvious, with spatial structures and order of magnitudes very consistent between the two satellite observations. As already mentioned for China, the OMI_{BISA} observations are larger than the GOME-2 columns in Northern mid-latitudes, mainly during the SON and DJF seasons.

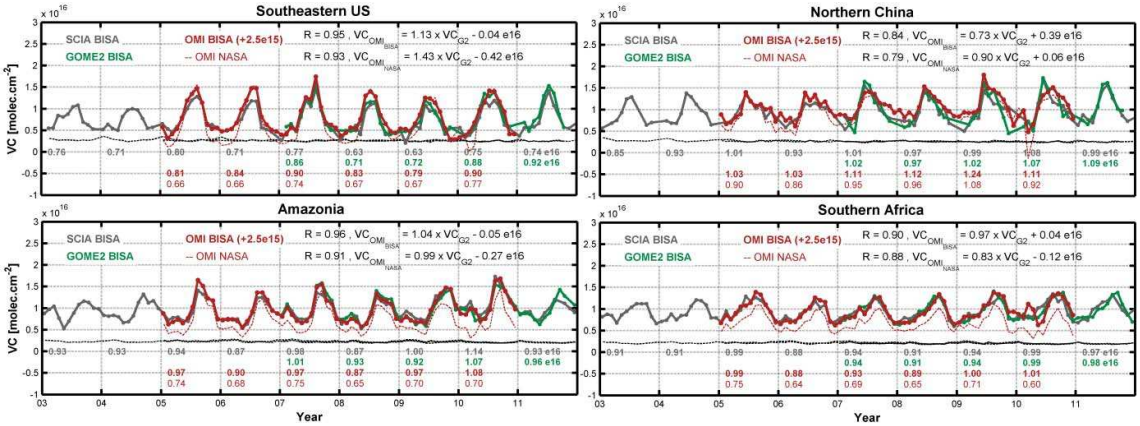

Figure 7: Regional averages of the SCIAMACHY, GOME-2 and OMI H_2CO H_2CO vertical columns, calculated over Southeastern US, Northern China, Amazonia and Southern Africa. Two versions are shown for OMI: the

VCs provided in the NASA product (OMI NASA, dotted red line), and the VCs calculated at BIRA-IASB (OMI BISA, red line) with AMF settings consistent with the SCIAMACHY and GOME-2 H_2CO products, and adding a continental offset of $2.5x10^{15}$ molec.cm^{-2}. The correlations and regression lines between each OMI product and the GOME-2 results are given inset. Annual values are given at the bottom of each subplot for each instrument [10^{16} molec.cm^{-2}].

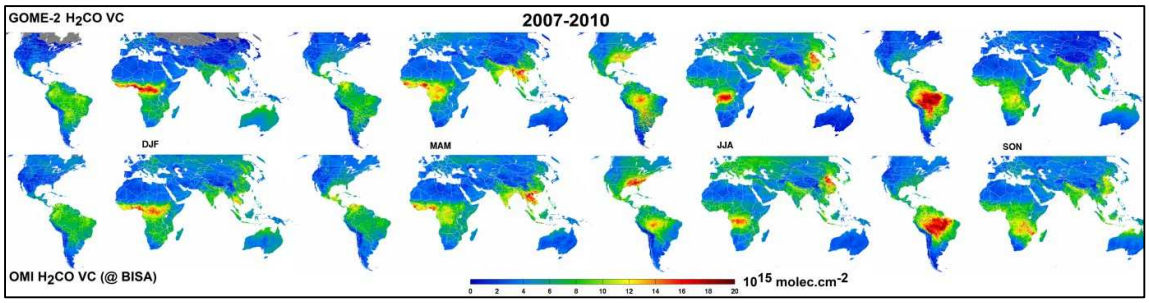

Figure 8: Seasonal maps of the H_2CO vertical columns, averaged over the 2007-2010 period, as retrieved from GOME-2 and OMI measurements (with BISA AMFs and continental offset).

5. GROUND-BASED OBSERVATIONS

Finally, we compare the remaining differences observed between the GOME-2 and OMI_{BISA} H_2CO vertical columns with ground-based measurements in the Beijing area. Indeed, as part of the AMFIC project (www.amfic.eu), BIRA-IASB operated a MAX-DOAS and direct sun instrument in Beijing, in collaboration with the Institute of Atmospheric Physics (IAP) of the Chinese Academy of Sciences (CAS). The system was located a few hundred meters from the Olympic stadium, and was continuously operated from July 2008 to April 2009. Since 2010, the system has been operated in Xianghe, located at 50 km east of Beijing.

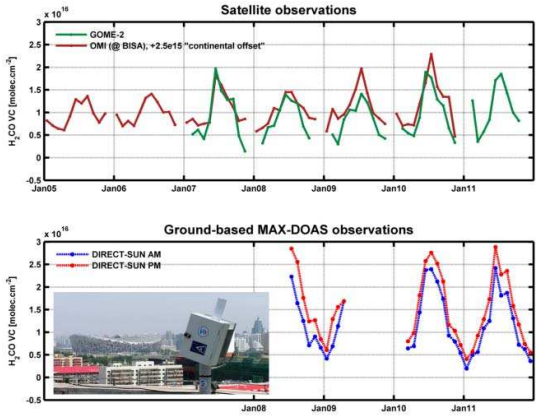

Figure 9: Monthly averaged H_2CO vertical columns observed with GOME-2 and OMI (upper panel), and direct-sun measurements (lower panel) in Beijing and Xianghe.

Figure 9 presents the GOME-2 and OMI_{BISA} H_2CO VCs in this region (upper panel), and the direct-sun observations (lower panel). The higher OMI observations (recorded around 01:30 pm) compared to the GOME-2 columns (recorded around 09:30 am) are partly explained by the differences observed between the morning and afternoon observations of the direct-sun measurements**.** The systematic differences between the satellite and ground-based H_2CO columns are explained by uncertainties in a priori profiles and by the vertical averaging kernels of the satellite observations.

CONCLUSIONS

We presented the first comparison of the GOME-2 and OMI formaldehyde products, for 4 years of coincident measurements between 2007 and 2010. These products are respectively available on the TEMIS and the NASA websites.

Each step of the retrievals was compared and new air mass factors were calculated for OMI with parameters consistent with GOME-2. The main differences were found to be related to a negative continental offset of the OMI slant columns compared to GOME-2, to the different wavelengths used to perform the radiative transfer calculations, and with a lesser extent, to the aerosol correction. After corrections of these differences, the final vertical columns agreed very well between GOME-2 and OMI in most of the regions. In Northern China however, the OMI H_2CO VCs are found to be systematically larger than the GOME-2 observations. This last feature is supported by ground-based direct-sun measurements performed in Beijing, showing larger H_2CO concentrations in the afternoon than in the morning.

These results are preliminary and need to be further studied. In particular, the impact of the different DOAS settings used to fit the slant columns need to be assessed. Furthermore, we need more ground-based measurement to resolve current uncertainties regarding the true H_2CO columns, and their diurnal

variations in various ecosystems and chemical regimes.

REFERENCES

De Smedt, I., Müller, J.-F., Stavrakou, T., van der A, R., Eskes, H. and Van Roozendael, M.: Twelve years of global observations of formaldehyde in the troposphere using GOME and SCIAMACHY sensors, Atmos. Chem. Phys., 8(16), 4947-4963, 2008.

De Smedt, I., Stavrakou, T., Müller, J. F., van Der A, R. J. and Van Roozendael, M.: Trend detection in satellite observations of formaldehyde tropospheric columns, Geophys. Res. Lett., 37(18), L18808, doi:10.1029/2010GL044245, 2010.

De Smedt, I., Van Roozendael, M., Stavrakou, T., Müller, J.-F., Lerot, C., Theys, N., Valks, P., Hao, N., and van der A, R.: Improved retrieval of global tropospheric formaldehyde columns from GOME-2/MetOp-A addressing noise reduction and instrumental degradation issues, Atmos. Meas. Tech. Discuss., 5, 5571-5616, doi:10.5194/amtd-5-5571-2012, 2012.

Kurosu, T. P., OMHCHO README FILE, http://www.cfa.harvard.edu/tkurosu/SatelliteInstruments/OMI/PGEReleases/READMEs/OMHCHO_README.pdf, last access: 14/08/2012, 2008.

Martin, R. V., Chance, K. V., Jacob, D. J., Kurosu, T. P., Spurr, R. J. D., Bucsela, E., Gleason, J. F., Palmer, P. I., Bey, I., Fiore, A. M., Li, Q., et al.: An improved retrieval of tropospheric nitrogen dioxide from GOME, J. Geophys. Res., 107(D20), doi:10.1029/2001JD001027, 2002.

Martin, R. V., Jacob, D. J., Yantosca, R. M., Chin, M. and Ginoux, P.: Global and regional decreases in tropospheric oxidants from photochemical effects of aerosols, J. Geophys. Res., 108(D3), 4097, doi:10.1029/2002JD002622, 2003.

Meller, R., and Moortgat, G. K.: Temperature dependence of the absorption cross section of HCHO between 223 and 323K in the wavelength range 225–375 nm, J. Geophys. Res., 105(D6), 7089–7102, doi:10.1029/1999JD901074, 2000.

Palmer, P. I., Jacob, D. J., Chance, K. V., Martin, R. V., D, R. J., Kurosu, T. P., Bey, I., Yantosca, R. and Fiore, A.: Air mass factor formulation for spectroscopic measurements from satellites: Application to formaldehyde retrievals from the Global Ozone Monitoring Experiment, J. Geophys. Res., 106(D13), 14539-14550, doi:10.1029/2000JD900772, 2001.

Platt, U. and Stutz, J.: Differential Optical Absorption Spectroscopy: Principles and Applications (Physics of Earth and Space Environments), Springer-Verlag, Berlin, Heidelberg, ISBN 978-3540211938, 2008.

Spurr, R. J. D.: LIDORT and VLIDORT: Linearized pseudo-spherical scalar and vector discrete ordinate radiative transfer models for use in remote sensing retrieval problems, in Light Scattering Reviews, edited by A. Kokhanovsky, pp. 229–271, Berlin, 2008.

Stammes, P., Sneep, M., de Haan, J. F., Veefkind, P., Wang, P. and Levelt, P. F.: Effective cloud fractions from the Ozone Monitoring Instrument: Theoretical framework and validation, J. Geophys. Res., 113(D16), D16S38, doi:10.1029/2007JD008820 [online] Available from: http://dx.doi.org/10.1029/2007JD008820, 2008.

Kleipool, Q. L., Dobber, M. R., de Haan, J. F. and Levelt, P. F.: Earth surface reflectance climatology from 3 years of OMI data, J. Geophys. Res., 113(D18), D18308, doi:10.1029/2008JD010290, 2008.

Wang, P., Stammes, P., van der A, R., Pinardi, G., and Van Roozendael, M.: FRESCO+: an improved O_2 A-band cloud retrieval algorithm for tropospheric trace gas retrievals, Atmos. Chem. Phys., 8, 6565-6576, doi:10.5194/acp-8-6565-2008, 2008.